THAPATHALI CAMPUS
Institute of Engineering
Tribhuvan University

Numerical analysis on stall suppression of a NACA 0012 airfoil by use of burst control plates

Ashim Chhetri[a,*], Sudip Bhattrai [a]

[a]Department Of Mechanical And Aerospace Engineering, Pulchowk Campus, Institute of Engineering, Tribhuvan University, Pulchowk, Lalitpur, Nepal

ARTICLE INFO

Abstract

Stall suppression is vital during takeoff, maneuver, and landing. Burst Control Plates (BCPs) suppress stall by creating vortices at the leading edge. To suppress stall on NACA 0012 (National Advisory Committee for Aeronautics) airfoil, rectangular cross-section BCPs of a constant height 0.005c and of five different widths (0.008c, 0.016c, 0.024c, 0.032c and 0.040c) are numerically analyzed at four different positions (0.045c, 0.05c, 0.07c and 0.1c) on airfoil using ANSYS FLUENT software with transition SST model. For this study airfoil of 200mm chord length (c) at Reynolds number (R_e) 1.3×10^5 is used. Coefficient of lift (C_L), coefficient of drag (C_D), and coefficient of pressure (C_P) are studied at different angles of attack (α) for various configurations. BCPs of thickness 0.032c and 0.040c located at 0.045c and 0.05c, suppressed stall by 4°. Other configurations suppressed stall by 2°. Stall suppression by BCP at 0.045c of a thickness 0.032c is found to be the most effective among various configurations.

1. Introduction

Control of flow separation can benefit in many ways such as improvement of lift/stall characteristics which lead to better performance due to a decrease in landing speed and increase in maneuverability, thereby widening the operating range of aircraft wings. Airfoil stall depends on the occurrence of a short bubble burst at the airfoil front section and separation of turbulent boundary layer at the airfoil rear section. The flow may reattach to the surface of the airfoil as a turbulent shear layer after the separation of laminar boundary layer from it. Laminar separation bubbles are used to describe the space between laminar separation and reattachment [1]. Controlling the flow around an airfoil to produce more lift and less drag is known as flow control. Techniques to delay separation of flow at the leading edge by stall control devices like pneumatic turbulators [2], boundary-layer trips [3], transition ramps [4], burst control plates, etc. control laminar separation bubble behavior. A burst

control plate can have a large application on unmanned aerial vehicles (UAV) with low speed but also has a major drawback due to the plate's placement in the airfoil's leading edge [5]. Thin burst control plates trailing edge can be used to create artificial vortices. They have an impact on the vortices that occur naturally within the laminar separation bubble (LSB), and as a result, even at an angle of attack where stalling of airfoil occurs, the reattachment of flow may take place at the airfoil surface [6].

Rinoie et.al. carried out the first investigation on short bubble burst control as a technique for preventing airfoil stall. One of the unique ideas was to intentionally control the formation of the separated shear layer by inserting a thin plate within the short bubble. Their experimental findings showed that the vortices developed at the plate trailing edge increase those created by Kelvin- Helmholtz disturbances within the split shear layer, which drives the divided shear layer to rejoin downstream of the plate. Due to which, the stall angle and maximum lift coefficient of NACA 0012 airfoil were also raised [6]. According to Kurita et al., applying

*Corresponding author:
✉ 076mstim002.ashim@pcampus.edu.np (A. Chhetri)

the plate with a rectangularcross-section to the same airfoil section was more successful than applying a thin plate, further suppressing the leading-edge stall due to the reattachment of circulating flow to the surface of airfoil approaching stall and modifying the characteristics of lift [7]. Grager et al. employed a "dynamic burst control plate" that oscillates the plate dynamically. They stated that this form of burst control plate efficiently suppresses stalls [8]. Nakamura et al. investigated the effect of leading edge and trailing edge position for burst control plates of rectangular cross-section with width, w/c=0.008 and height, h/c=0.005, for stall suppression, and found the best position with respect to the leading edge of the airfoil to be $X_p/c = 0.050$ [9]. Another study by Shrestha et al. found the best possible height of BCPs for NACA 0015 airfoil, which is found to be 0.05c at 0.2c position for best stall suppression [10].

Despite the fact that many researchers have investigated BCPs, detailed studies for the best possible width of BCPs still have not been studied. The width of BCPs plays a vital role in the formation of vortical structures that shorten the short bubbles and in the design optimization leading to changes in weight, and skin drag. So, finding the effect of the width of BCPs and the best possible width is a vital part of this research. For this research, the impact of the BCPs width on a NACA 0012 airfoil was numerically analyzed.

2. Computational Method

The influence of the BCPs width at different positions on the stall angle of NACA 0012 airfoil is studied numerically. The two-dimensional Reynolds-Averaged Navier-Stokes (RANS) equations are numerically solved to determine the flow field around the airfoil. Transition SST, the k-ω SST model, the Realizable k-ϵ model, and the one-equation S-A models are four models of turbulence tested numerically by Shrestha et al. and found out Transition SST, the best model for investigating drag and lift coefficient at low Reynolds number for the airfoil [10]. So, the Transition SST model is used in this study.
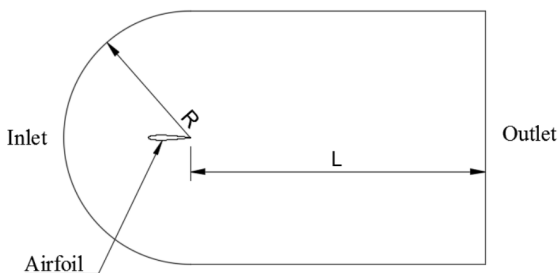

Figure 1: The C-type computational domain

Fluent software was used to perform numerical calculations. A C-type 2D computational domain was designed for the study. Figure 1 shows the computational domain which has downstream length (L) = 30c and radius (R) = 15c. The airfoil has a 200 mm chord (c) length.

2.1. Computational mesh, boundary conditions, and solver setup

As illustrated in Figures 2, 3, 4 a structured mesh was employed over the whole computational domain once the computational mesh was constructed using the program ANSYS Fluent. There were approximately 408,400 cells in the entire computational domain. The airfoil and BCP surface's first mesh layer height was 3.1×10^{-5} m. These heights satisfy the computational criteria of the chosen turbulence model by having a y value smaller than 1.
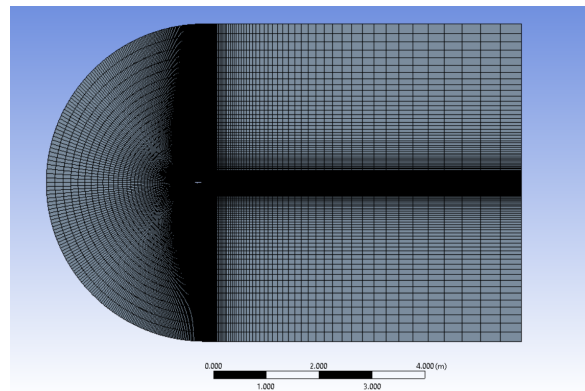

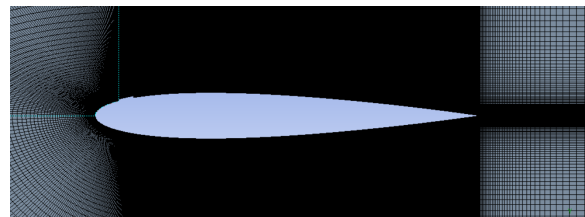Figure 2: Structured grid of computational domain
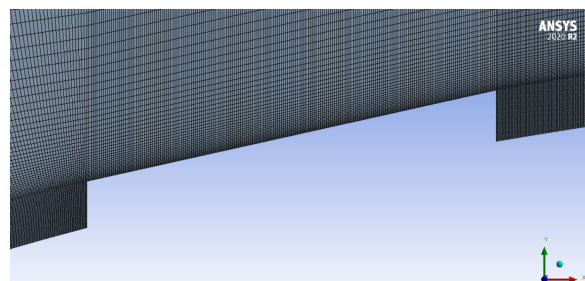

Figure 3: Dense grid near airfoil surface

Figure 4: Dense grid near airfoil surface

The computational domain's front, upper, and bottom boundaries were set as velocity inlets, the back boundary as a pressure outlet, and the airfoil boundary as a no-slip wall. The Transition SST turbulence model was selected as suggested in [10]. The solver has a steady state setting. The solver adopted is pressure based as the flow is assumed to be incompressible. Pressure, viscosity, and density are taken into account as they would be at sea level. At 1%, the turbulence intensity is set. To obtain the appropriate Reynolds number (R_e) and value of y less than 1, the input freestream velocity was predetermined and set to 9.45 m/s. Pressure-velocity coupling algorithm SIMPLE (semi-implicit method for pressure-linked equations) and finite volume approach for discretizing RANS equations were used. The calculation uses second-order upwind spatial discretization. Cell-based least squares are used to choose the spatial gradient. Target values for residual convergence criterion were set at 10^{-7}.

Rectangular BCP is best for stall suppression than other plates [7]. Figure 5 shows a schematic diagram of the rectangular burst control plate geometric parameters. For all widths (w) and positions, the burst control plate of rectangular cross-section utilized in the current study has a constant height (h) along the direction of wing span. The chord-wise distance (shown as X_P) between the front end of the plate and the leading edge of the airfoil determined where the plate should be placed. Note that the distance along the X_C chord line of the airfoil was used to define X_P.
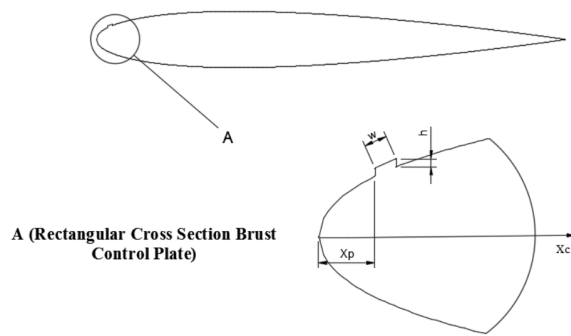

Figure 5: Geometric parameters for BCP with rectangular cross-section

According to Shrestha et al., the best height for stall suppression of BCP is 0.005c [10]. Different BCP positions that were employed for the experimental analysis in [9] are used for this study. A width of 0.032c was experimentally tested in [7] and width of 0.008c was experimentally tested in [9], but the effect on stall by variation in BCP width was not studied. So, present study focuses on width (0.008c, 0.016c, 0.024c, 0.032c and 0.04c)

which include the widths of previous experimental studies with small increment. Table 1 shows the geometric parameters for BCPs of constant height 0.005c tested for varying width ranging from 0.008c to 0.040c at various position ($X_p/c = 0.045, 0.05, 0.07, 0.1$) from the leading edge of NACA 0012 airfoil at different angles of attack.

Table 1: BCPS GEOMETRIC PARAMETERS.

Height (H)	Width (W)	Chord wise leading edge plate distance(X_P)
0.005c	0.008c	0.045c
	0.016c	0.05c
	0.024c	0.07c
	0.032c	0.1c
	0.040c	

Airfoil coefficient of lift (C_L) and coefficient of drag (C_D) are define by Equation 1 and Equation 2, respectively:

$$C_L = \frac{F_L}{\frac{1}{2}\rho V_\infty^2 L} \tag{1}$$

$$C_D = \frac{F_D}{\frac{1}{2}\rho V_\infty^2 L} \tag{2}$$

Where F_D and F_L are the airfoil total drag force and total lift force; air density (ρ) = 1.225 kg/m^3; velocity of freestream (V_∞) = 9.45 m/s; and airfoil's chord length (L) = 200 mm.
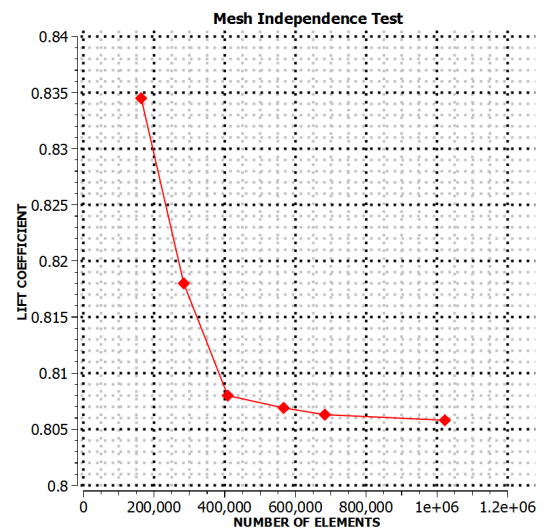
2.2. Grid Indepedence Study

Figure 6: Lift coefficient versus number of elements at $\alpha = 8°$

In order to test grid independence, six different meshes with increasing number of elements were utilized: 163,600 cells, 284,000 cells, 408,400 cells, 566,400 cells, 683,000 cells and 1,022,393 cells for the airfoil with BCP of width 0.040c at position 0.1c with an angle of attack (α) = 8°. Figure 6 shows a numerically obtained lift coefficient at $R_e = 1.3 \times 10^5$ for all sets, and the error percent of lift coefficient for 408,400 cells was found to be less than 1. So, 408,400 mesh was used for computation in this paper.

Three mesh qualities were tested: Skewness, Jacobian Ratio, and Orthogonal Quality. Mesh obtained has average skewness quality of 8.8316 e^{-2} an average Jacobian Ratio of 1.0032, and average Orthogonal Quality of 0.97682.

2.3. Model Validation

Flow field over NACA 0012 airfoil with BCP of width 0.032c at X_P 0.045c was numerically simulated using the Transition SST model. Figure 2(g) shows computed lift coefficients (C_L) values at different angles of attack ranging from 0° to 16° with an increment of 2° compared with clean airfoil and the experimental data of Nakamura et al. [7] at Reynolds number of 1.3×10^5. The average error percent of lift coefficient was found to be 9.847 % which is less than 10 % that falls under the acceptance region.
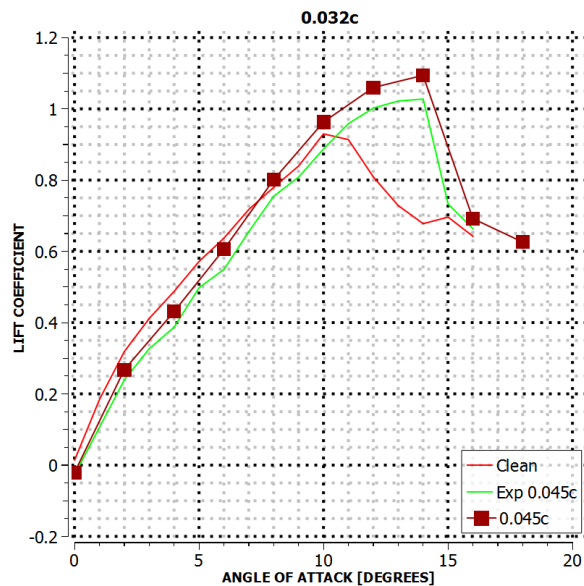

Figure 7: Lift coefficient versus angle of attack

3. Results and Discussion

Various sizes BCPs at different positions were used in the computations to examine the effect on flow around NACA 0012 airfoil. At 0.045c, 0.05c, 0.07c, 0.1c from

the leading edge of NACA 0012 airfoil, five BCPs with widths of 0.008c, 0.016c, 0.024c, 0.032c and 0.040c were examined.
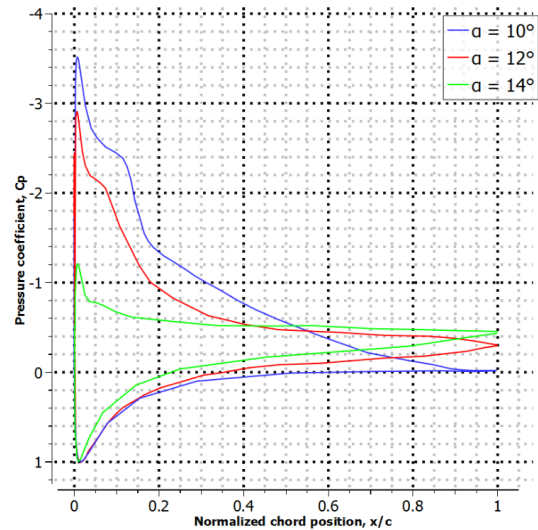

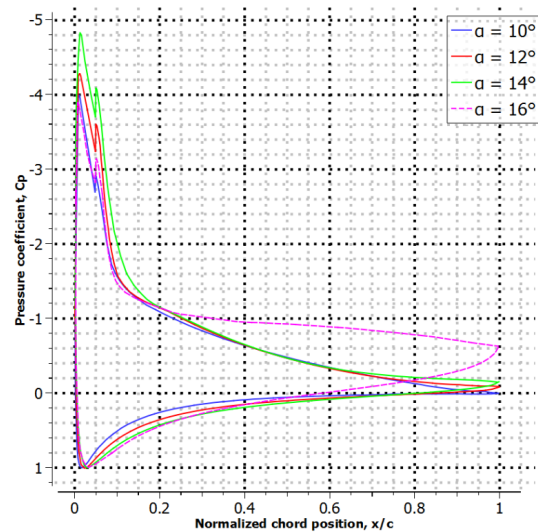Figure 8: C_P distribution along chord for clean airfoil

Figure 9: C_P distribution along chord for airfoil with 0.032c width BCP at 0.045c location

Figures 8 and 9 illustrate the distribution of pressure along the surface of a clean airfoil and an airfoil with BCP positioned at 0.045c and of width 0.032c respectively. With the clean airfoil for $\alpha = 10°$, the figure shows that a short bubble was created (note toward the leading edge of airfoil the strong suction pressure, succeed by a flat area and sharp recovery of pressure, which denotes flow reattachment). With the clean airfoil, when α was raised from 10° to 12°, there is a loss of coefficient of pressure, indicating that the airfoil has stalled.

When α was raised to 14° for this airfoil, both the strong suction pressure toward the leading edge of airfoil and sharp recovery of pressure were completely removed. At $\alpha = 14°$, a high suction pressure peak was seen for the airfoil with BCP, indicating stall suppression. Figures also indicate that for the same angle of attack, an airfoil with BCP has reduced coefficients of pressure (C_P) when compared to a clean airfoil. A sharp rise in coefficients of pressure (C_P) at chord position 0.05c indicates a sudden decrease in pressure due to the presence of BCP.

The lift coefficients of clean NACA 0012 airfoil and same airfoil with BCPs of widths 0.008c, 0.016c, 0.024c, 0.032c and 0.040c positioned with respect to the leading edge at 0.045c, 0.05c, 0.07c and 0.1c of the airfoil are shown in Figures 10, 12, 14, 16 and 18. When the angle of attack is less than 6°, airfoil with BCPs shows lower C_L than clean airfoil for all widths at all positions. Between 6° and 18° airfoil with BCPs shows a greater value of C_L. At maximum stall angle $\alpha = 14°$ for BCP of width 0.04c at the location X_P 0.05c, the maximum lift coefficient is 1.129, which is over 21.42% greater than the maximum lift coefficient of the clean airfoil (0.92978) at $\alpha = 10°$ for $R_e = 1.3 \times 10^5$. Stall angle is suppressed to 14° for an airfoil with BCPs width 0.032c at X_P 0.045c and 0.05c and width 0.04c at X_P 0.045c and 0.05c. For the rest of the BCPs width at different locations, the stall angle is suppressed to 12°. The position that produced the highest lift for each BCPs width was observed to be at 0.05c. This might be because at the downstream of flow, the separated flow reattaches and the LSB's size is shortened as a result of the re-energized separated boundary layer.

The drag coefficients of clean airfoil and BCPs with widths of 0.008c, 0.016c, 0.024c, 0.032c and 0.040c positioned at 0.045c, 0.05c, 0.07c, 0.1c with respect to the leading edge are shown in Figures 11, 13, 15, 17 and 19. At angles of attack less than 8°, C_D is more for BCPs of all widths at all positions when compared to the airfoil with no BCPs. This increase in drag is due to skin friction. Drag is effectively reduced when the angles of attack are between 8° and 18° for all BCPs at all positions. At $\alpha = 14°$, the minimum coefficient of drag is 0.0745 for BCP width 0.032c at position 0.045c, which compared to clean airfoil is 10.024 % reduction in drag. At $\alpha = 12°$, the minimum coefficient of drag is 0.046 for BCP width 0.008c at position 0.1c, which compared to clean airfoil is 44.44 % reduction in drag. As the angle of attack increases, drag coefficient steadily rises as the separation of turbulent boundary layer at the back of the airfoil moves upstream. Drag coefficients for all configurations converge at $\alpha = 18°$ with the clean airfoil case.
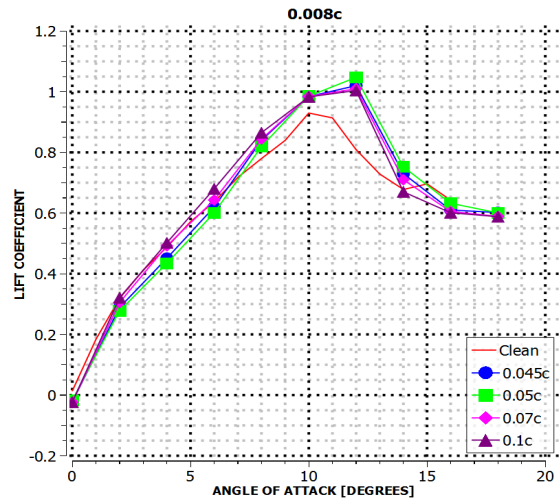

Figure 10: Lift coefficient versus angle of attack
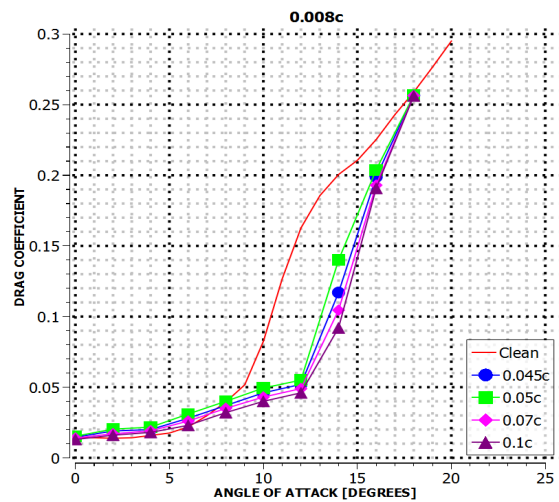

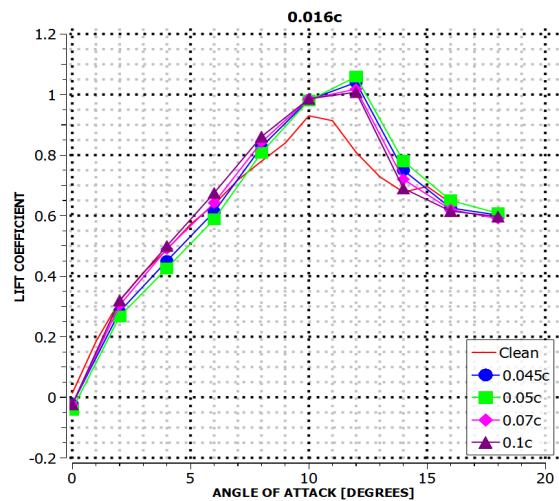Figure 11: Drag coefficient versus angle of attack

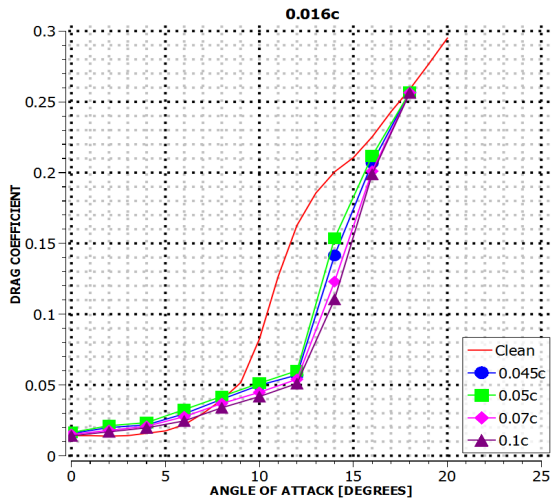Figure 12: Lift coefficient versus angle of attack

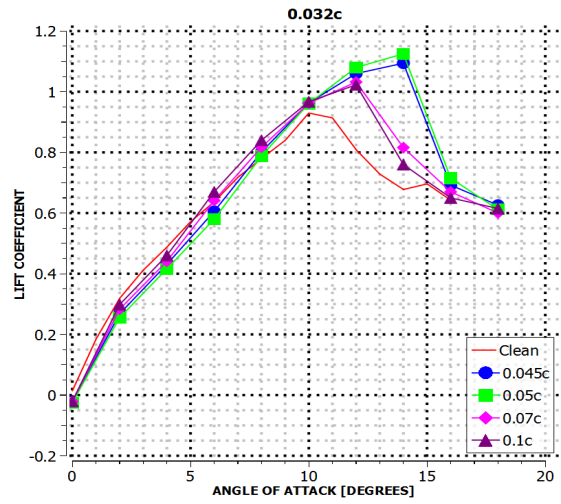Figure 13: Drag coefficient versus angle of attack

Figure 16: Lift coefficient versus angle of attack
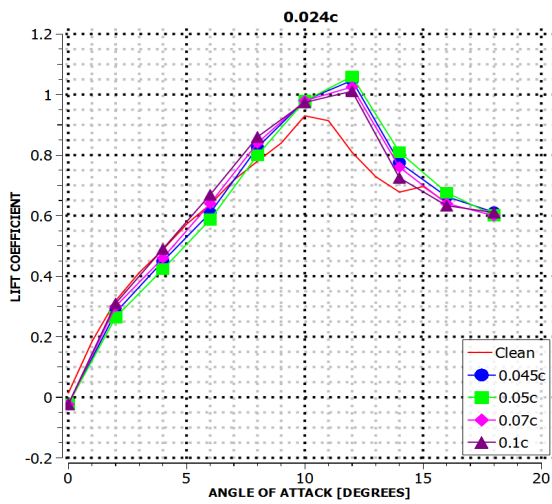

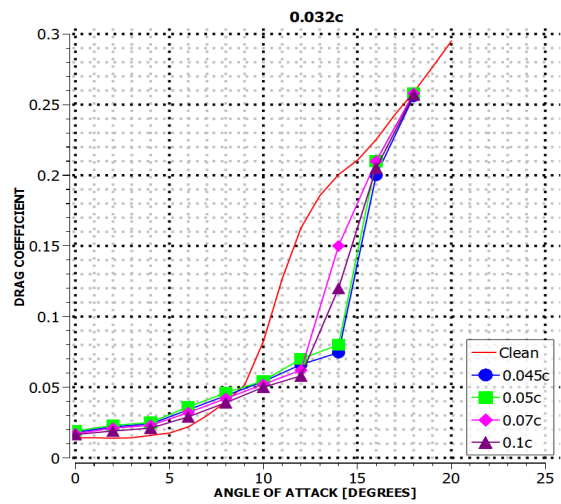Figure 14: Lift coefficient versus angle of attack

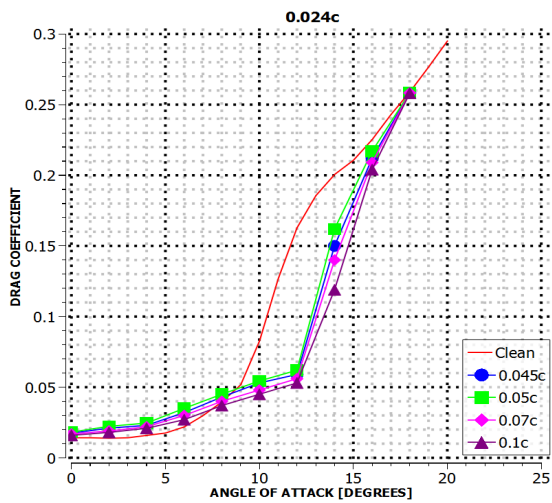Figure 17: Drag coefficient versus angle of attack

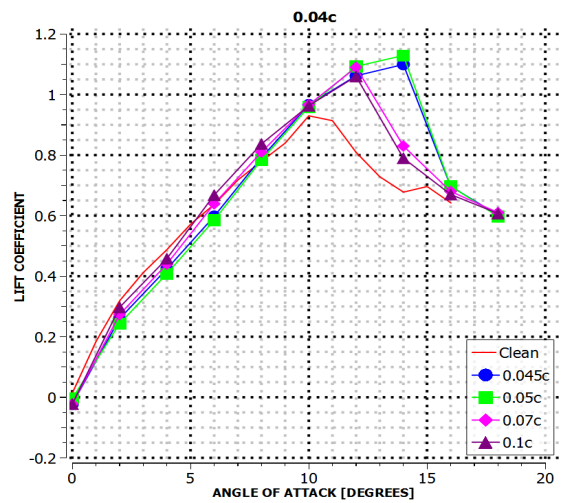Figure 15: Drag coefficient versus angle of attack

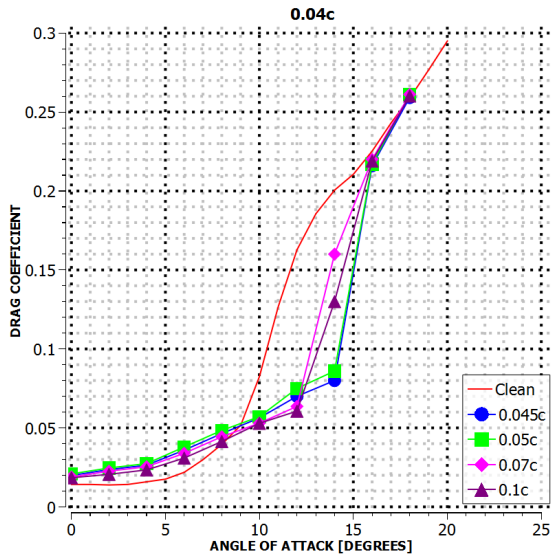Figure 18: Lift coefficient versus angle of attack

0.04c

Figure 19: Drag coefficient versus angle of attack

Figure 20 illustrates the lift coefficients of BCPs width of 0.008c, 0.016c, 0.024c, 0.032c, and 0.040c positioned at 0.05c with respect to the airfoil leading edge and compared with clean airfoil at various angles of attack. Results show that for angles of attack less than 8°, C_L are lower than clean airfoil for an airfoil with BCPs. When angles of attack are greater than 8°, the lift coefficients for all cases are larger than those of clean airfoil. The maximum lift coefficient among above configurations is shown by airfoil with BCP width 0.04c at 0.05c for angles of attack between 8° to 18°. At $\alpha = 18°$, all configurations C_L reattach with C_L of clean airfoil.
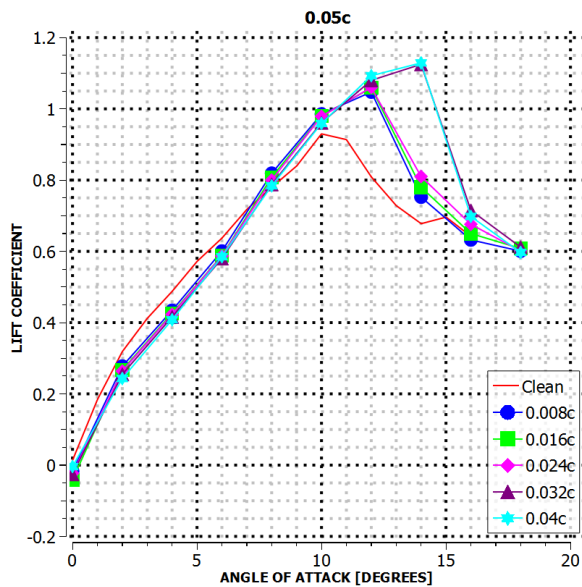
0.05c

Figure 20: Lift coefficient versus angle of attack

Figure 21 illustrates coefficients of drag for BCPs of width 0.008c, 0.016c, 0.024c, 0.032c and 0.040c positioned at 0.05c with respect to the airfoil leading edge and compared with clean airfoil at various angles of attack. Among above configurations that have suppressed stall angle by 4° than clean airfoil, the minimum drag coefficient is shown by airfoil with BCP width 0.032c at 0.045c for angles of attack between 8° to 18°. C_D is greater than clean airfoil for all configurations at angles of attack less than 8°.
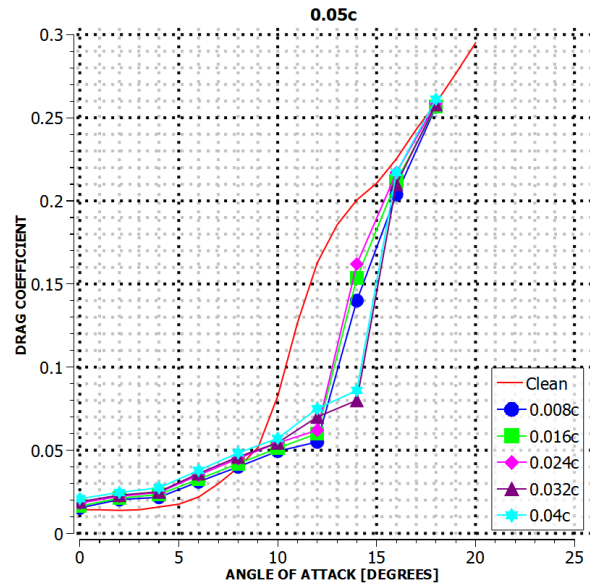
0.05c

Figure 21: Drag coefficient versus angle of attack

4. Conclusion

In this study, ANSYS Fluent software was used to simulate BCPs (with five different widths of 0.008c, 0.016c, 0.024c, 0.032c, and 0.040c and constant height 0.005c) added on NACA 0012 airfoil and the effect of widths on stall suppression at the low Reynolds number of 1.3×10^5 was studied. The coefficient of lift and the coefficient of drag were studied for different configurations at different angles of attack (from 0° to 18°) to determine the stall angle and sliding ratio. Among various configurations studied, BCP of width 0.032c and 0.04c at positions 0.045c and 0.05c did maximum stall suppression of 4° (from 10° to 14°). The maximum sliding ratio (C_L/C_D) at an angle of attack of 14° is 14.68 which is shown by BCP of width 0.032c positioned at 0.045c with respect to the airfoil leading edge is found to be the best. For BCPs position 0.07c and 0.1c with respect to the airfoil leading edge, all width of BCPs shows the same stall angle of 12°. For BCPs position 0.045c and 0.05c with respect to the airfoil leading edge, 0.032c and 0.04c width BCPs show stall

angle of 14°, and other widths of BCPs show the same stall angle of 12°. So BCPs of high thickness are more effective to suppress stall when close to the airfoil leading edge. It is due to the perfect vortex height created in front of BCPs which is equal to BCPs height and the reduction in the size of laminar separation bubble at the back of BCPs, leading to fast flow reattachment. It is recommended for experimental analysis of this research to validate the result. For the better study of physics and to visualize the flow around the airfoil with burst control plates of various widths and locations, a particle image velocimetry (PIV) system is recommended for further study. Few sizes and positions of rectangular burst control plates were studied due to time limitations. So, it is recommended to study for large configurations and to test at fine angles of attack for more accurate results. The shape of burst control plate also affects the flow pattern and size of laminar separation bubble. Different cross sections like circular, triangular, etc. of burst control plate can be used for further study.

References

[1] Tani I. Low-speed flows involving bubble separations[J/OL]. Progress in Aerospace Sciences, 1964, 5: 70-103. DOI: https://doi.org/10.1016/0376-0421(64/90004-1.

[2] Pfenninger W, Vemuru C S. Design of low reynolds number airfoils[J/OL]. Journal of Aircraft, 1990, 27(3): 204-210. DOI: 10.2514/3.45920.

[3] Van Ingen J L, Boermans L M M. Aerodynamics at low reynolds numbers: A review of theoretical and experimental research at delft university of technology[C]// Proceedings of Aerodynamics at Low Reynolds Numbers Conference: volume 1. Royal Aeronautical Society, 1986: 1.1-1.40.

[4] Eppler R, Somers D M. Airfoil design for reynolds numbers between 50,000 and 500,000[C]// Proceedings of Low Reynolds Number Airfoil Aerodynamics Conference. Notre Dame, IN: University of Notre Dame, 1985: 1-14.

[5] Wong C W, Rinoie K. Bubble burst control for stall suppression on a naca 631-012 airfoil[J]. Journal of aircraft, 2009, 46(4): 1465-1468.

[6] Rinoie K, Okuno M, Sunada Y. Airfoil stall suppression by use of a bubble burst control plate[J/OL]. AIAA Journal, 2009, 47 (2): 322-330. DOI: 10.2514/1.37352.

[7] Kurita S, Rinoie K, Sunada Y. Stall suppression by use of a rectangular cross section plate placed on naca0012 airfoil[C]// for Aeronautical J S, Sciences S. Proceedings of the 40th Fluid Dynamics Conference. Tokyo, 2008: 331-334.

[8] Grager T, Rothmayer A, Hu H. Stall suppression of a low-reynolds-number airfoil with a dynamic burst control[J]. AIAA Paper, 2011: 2011-1180.

[9] Nakamura Y, Rinoie K, Sunada Y. Airfoil stall suppression by use of rectangular cross section burst control plates[J]. In 50th AIAA Aerospace Sciences Meeting including the New Horizons Forum and Aerospace Exposition, 2012, 50: 318.

[10] Shrestha B, Bhattarai N. Numerical simulation studies on stall suppression of a naca0015 airfoil[J/OL]. Journal of Advanced College of Engineering and Management, 2021, 6: 23-31. DOI: https://doi.org/10.3126/jacem.v6i0.38276.